13

Influence of magnetron sputtering modes on properties of protective Ti-Al-Ta-N coatings

© A.Yu. Derbin, A.R. Shugurov, E.D. Kuzminov, A.V. Panin

Institute of Strength Physics and Materials Science, Siberian Branch, Russian Academy of Sciences, 634055 Tomsk, Russia

e-mail: derbinalexei@yandex.ru

Received January 28, 2025 Revised March 12, 2025 Accepted March 27, 2025

Applying of protective coatings is an effective way to increase the resistance of various parts and components against wear, oxidation and corrosion. In this article a comparative analysis of Ti-Al-Ta-N coatings deposited by high-power impulse magnetron sputtering and direct current magnetron sputtering is carried out. It is shown that the use of the combined sputtering mode can significantly increase the deposition rate. The influence of the deposition modes and the multilayer architecture of these coatings on their mechanical and tribological characteristics, as well as oxidation resistance, is investigated. It is established that optimization of the architecture of the Ti-Al-Ta-N multilayer coatings makes it possible to increase their hardness and wear resistance, but it has almost no effect on their oxidation resistance

Keywords: Ti-Al-Ta-N coatings, magnetron sputtering, mechanical properties, oxidation resistance.

DOI: 10.61011/TP.2025.08.61743.12-25

Introduction

The compound Ti-Al-Ta-N is considered to be one of the most promising four-component compositions designed to create protective wear-resistant coating that can replace the TiN and Ti-Al-N coatings which are widely used in many fields of science and technology. initio calculations have shown that introducing Ta into the Ti-Al-N metal sublattice provides higher occupancy of the $d-t_{2g}$ states near the Fermi level, increasing metallicity of interatomic bonds in the Ti-Al-Ta-N solid solution, and thereby improving its plasticity [1-4]. A shift in the Ti-Al-Ta-N solid solution results in formation of a lamellar electron structure that consists of alternating layers of high and low charge density in the metal sublattice, which makes it possible to selectively react to normal and shift stresses [1]. The calculations have also shown a growth of cohesion energy of the solid solution with increase of the Ta content [2]. The experimental studies confirmed increase of fracture resistance of the Ti-Al-Ta-N coatings while maintaining high hardness [4-6]. Besides, change of an electron structure caused by introduction of the Ta atoms as well as higher energy of activation of Ta diffusion in comparison with Ti and Al suppress spinoidal decomposition of the Ti-Al-Ta-N solid solution and formation of the AIN hexagonal phase (wurtzite) at the temperatures below 1200 °C [2], thereby resulting in increase of thermal stability of the coatings. The Ti-Al-Ta-N coatings also have excellent oxidation resistance [2,7,8], which is explained by suppression of phase transformation anatase-rutile in a Ta-enriched oxide layer [7] and hindrance of diffusion of oxygen in this layer due to reduction of a number of oxygen vacancies [8].

However, despite the above-described excellent properties of the Ti-Al-Ta-N coatings, their columnar microstructure that is usually formed during physical deposition from a vapor phase [5-7,9-11] has a negative effect on their reliability and durability in many applications. First of all, boundaries of columnar grains, which are characterized by a lesser atomic density, facilitate propagation of through cracks in the coatings, which result in fracture of the coatings [12,13]. Secondly, at higher temperatures these boundaries ensure fast diffusion of oxygen inward the coatings, thereby facilitating oxidation of the coating and the substrate [14]. Finally, the columnar structure promotes diffusion of chemical elements of the coatings, thereby reducing its thermal stability [15].

The previous studies [16] have shown that using the highpower impulse magnetron sputtering (HiPIMS) method that is characterized by short powerful impulses with a frequency up to 10 kHz and high peak power density made it possible to suppress a growth of the columnar grains in the Ti-Al-Ta-N coatings and contributed to formation of their denser and more uniform microstructure. This effect is caused by a high portion of ions in a total flux of sputtered particles, which is achieved during HiPIMS, thereby providing more intense bombardment of the growing coatings with low-energy ions [17,18]. However, the HiPIMS method is characterized by lower sputtering rates in comparison with traditionally used methods, in particular, direct current magnetron sputtering (DCMS), which increases energy costs and reduces economic efficiency of coating production. In this regard, the aim of the present study was to investigate a possible increase of the rate of sputtering of the Ti-Al-Ta-N coatings with the dense microstructure by applying multilayer compositions by means of a combined

Designation of the coating batch	Architecture of the coatings	Sputtering mode	Thickness of the coatings, μm	Thickness of the layers, μm
D	Monolith	DCMS		_
Н	Monolith	DCMS		_
HD2	2-layer	HiPIMS/DCMS	3.0 ± 0.1	1.5
HD4	4-layer	HiPIMS/DCMS		0.75
HD6	6-layer	HiPIMS/DCMS		0.5
DH6	6-layer	HiPIMS/DCMS		0.5

Table 1. Architecture and modes of sputtering of the Ti-Al-Ta-N coatings

sputtering method, in which the HiPIMS and DCMS modes alternate.

1. Materials and methods

The coatings were applied by means of the magnetron sputtering system that is fitted with a round planar magnetron with a Ti-Al alloy target (50 at.% Ti, 50 at.% Al) with Ta inserts (99.99 at.%). The coatings based on the Ti-Al-Ta-N system were deposited in a medium of a mixture of argon and nitrogen gases at the operating pressure of 0.3 Pa in the vacuum chamber. During sputtering, a substrate holder located at the distance of 9 cm from the magnetron and heated from the temperature of 425 °C was energized with the bias voltage $U_b = -100 \,\mathrm{V}$. During HiPIMS, the coatings were deposited at a filling ratio of 10% (a ratio of duration of the negative impulse to the period) and an impulse repetition rate of 5 kHz. Thus, duration of the negative impulse, at which the target was sputtered, was $20 \mu s$. The coatings were deposited onto substrates made of AISI 321 steel the Ti-6Al-4V titanium alloy and Si (100). The steel substrates were used to study an elementary composition as well as mechanical properties and wear resistance of the coatings. coatings on the Ti-6Al-4V substrates were designed for X-ray diffraction studies and thermal tests. The coatings on silicon were used for studying a microstructure of cross sections and measuring residual internal stresses. The substrates made of AISI 321 and Ti-6Al-4V were prepared by spark cutting as rectangular plates with the sizes $15 \times 10 \times 1.5$ mm³. Before deposition of the coatings, these substrates were mechanically ground and polished to mirror shine. The silicon substrates were shaped as square plates of the size $10 \times 10 \times 0.7 \,\mathrm{mm}^3$. Before being loaded into a vacuum chamber, all the substrates were cleaned in alcohol for 20 min using an ultrasonic bath. After that, for additional cleaning, they were bombarded by the Ar+ ions in the vacuum chamber for 20 min. Before applying the coatings to the substrate, a TiAl adhesion sublayer was applied to the substrates of the thickness of 30 nm by magnetron sputtering before application of the coatings.

The 6 batches of the Ti-Al-Ta-N coatings (Table 1) were prepared and investigated: the monolith coatings applied by direct current magnetron sputtering (hereinafter referred to as D) and high-power impulse magnetron sputtering (hereinafter referred to as H) as well as the coatings that consisted of 2, 4 and 6 alternating HiPIMS and DCMS layers. In the 2- and 4-layer coatings (hereinafter referred to as HD2 and HD4, respectively), the first layer was applied by HiPIMS, whereas in case of the 6-layer coatings two sample options were studied: with the HiPIMS first layer (designated as HD6) or with the DCMS first layer (designated as DH6). The total thickness of all the coatings as well as the thicknesses of separate layers are given in Table 1.

The elementary composition of the coatings was determined by energy-dispersive X-ray spectroscopy in the scanning electron microscope EVO 50 equipped with the Inca X-Act detector. A structure and a phase composition of the coatings were studied by X-ray diffraction in the appliance Shimadzu XRD-7000. The studies were performed using CuK_{α} -radiation in conditions of symmetrical shooting. An average size of the coherent scattering regions d in the Ti-Al-Ta-N coatings was calculated by means of the Scherrer relationship [19]:

$$d = K\lambda/(\beta\cos\theta),$$

where K — the Scherrer constant, λ — the wavelength of X-ray radiation, β — the reflection width at half maximum, θ — the diffraction angle. The coating microstructure was studied by investigating cross sections by scanning electron microscopy (SEM). Hardness H and the reduced Young's modulus E^* of the coatings were determined by nanoindentation in a NanoTest installation using a Berkovich diamond indenter. The measurements were carried out by controlling an applied load, whose maximum value was 20 mN. The residual stresses σ_f that develop in multilayer coatings on the silicon substrates were estimated using the Stoney equation [20]:

$$\sigma_f = E_s d_s^2 / (6R(1 - v_s)d_f),$$

where E_s — the Young's modulus of the substrate material; d_s — the substrate thickness; R — the radius of substrate

bending; ν_s — the Poison's ratio of the substrate material; d_f — the film thickness. The measurements were carried out using the contact profilometer Alpha-Step IQ.

Wear of the Ti-Al-Ta-N coatings was estimated by tribological tests in a ball-on-disc scheme in conditions of dry friction at the room temperature by means of the tribometer CSEM CH2000. The counterbody was a ball that was made of the WC8 alloy and had a diameter of 6 mm. The track radius was 2.5 mm, the travelling speed was 25 mm/s, the load was 1 N, the friction path was 100 m. Damage accumulation on a surface of the tribotracks was analyzed by SEM. Volume wear of the coatings was determined by measuring cross-section profiles of the tribotracks using the contact profilometer Alpha-Step IQ.

The samples were thermally annealed in the tubular muffle furnace SNOL 0.8/1250 in air atmosphere at the temperature of 950 °C. The heating rate was 30 K/min, while the cooling rate was $\sim 50\, \text{K/min}.$ The annealing duration was 5 h.

2. Results and discussion thereof

Fig. 1 shows the deposition rate of the Ti-Al-Ta-N coatings produced in the various modes of magnetron sputtering. It can be seen that the deposition rate of the H coating is reduced by a factor of two as compared to the D coatings. It is caused by self-sputtering of the growing coatings in the HiPIMS mode due to intense ion bombardment as well as return of a part of the sputtered ions back to the target surface. Both the effects are caused by a high degree of ionization of sputtered particles in the HiPIMS mode [17]. In turn, using a combination of the HiPIMS and DCMS modes allowed increasing the deposition rate of the Ti-Al-Ta-N coatings deposited onto substrates made of AISI 321 steel as compared to the HiPIMS mode.

The elementary composition of the Ti-Al-Ta-N coatings was studied by energy-dispersive spectroscopy

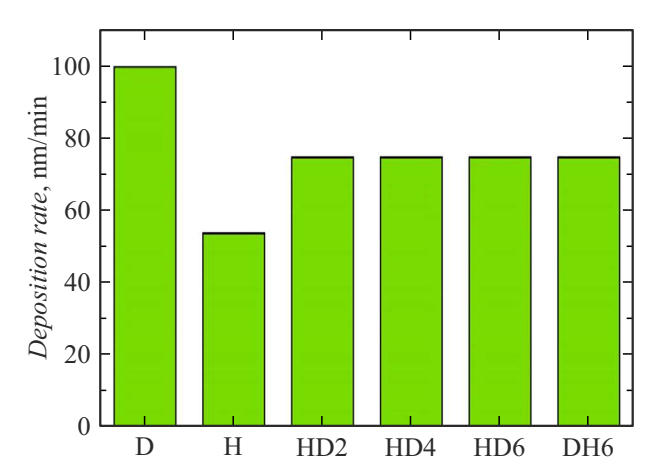


Figure 1. Deposition rate of the Ti-Al-Ta-N coatings produced in the various modes.

Table 2. Content of Ti, Al and Ta in the Ti-Al-Ta-N coatings produced in the various modes

Designation of the coating batch	Ti, at.%	Al, at.%	Ta, at.%
D	45.6	43.2	11.2
Н	47.2	41.3	11.6
HD2	45.2	43.4	11.4
HD4	45.6	43.5	10.9
HD6	45.9	43.1	10.9
DH6	46.8	42.2	11.0

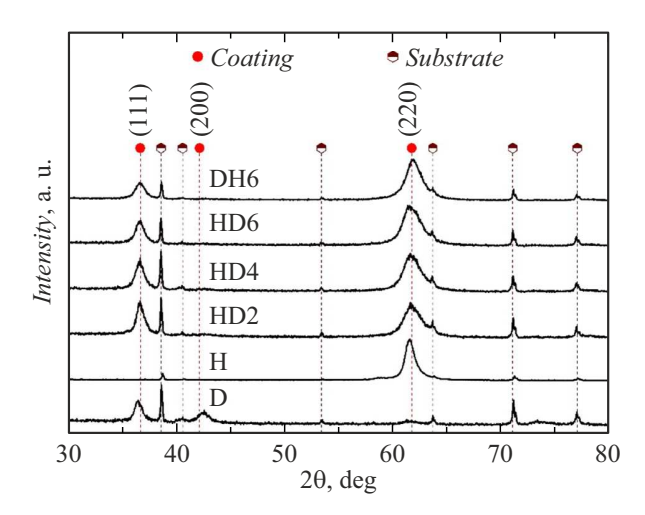


Figure 2. Diffraction patterns of the Ti-Al-Ta-N coatings produced in the various modes.

to show that the content of Ta slightly depended on the sputtering mode and was ~ 11 at.% (Table 2). At the same time, the H coatings exhibited noticeably more Ti and less Al than in the D coatings. The main reason for this is more intense self-sputtering of the growing coatings in the HiPIMS mode due to increase of the number of ions in the total flux of particles incident to the substrate. Since light atoms sputter with greater probability than heavy atoms, the content of Al, whose atoms are the lightest among the metals included in the Ti-Al-Ta-N coatings, is reduced as compared to the heavier Ti and Ta atoms. In the multilaver coatings, the content of the elements is determined by a chemical composition of separate layers and their arrangement in relation to a free surface. Therefore, in the majority of the multilayer coatings the elementary composition is close to the D coatings, whereas in the DH6 samples that have the HiPIMS layer at the top the content of the elements is almost the same as in the H coatings.

Fig. 2 shows X-ray diffraction patterns obtained for the studied Ti-Al-Ta-N coatings. The diffraction patterns were analyzed to show that all the coatings were the Ti-Al-Ta-N solid solution with a single-phase FCC structure of the B1 type (NaCl). At the same time, the D coatings have no pronounced predominant crystallite

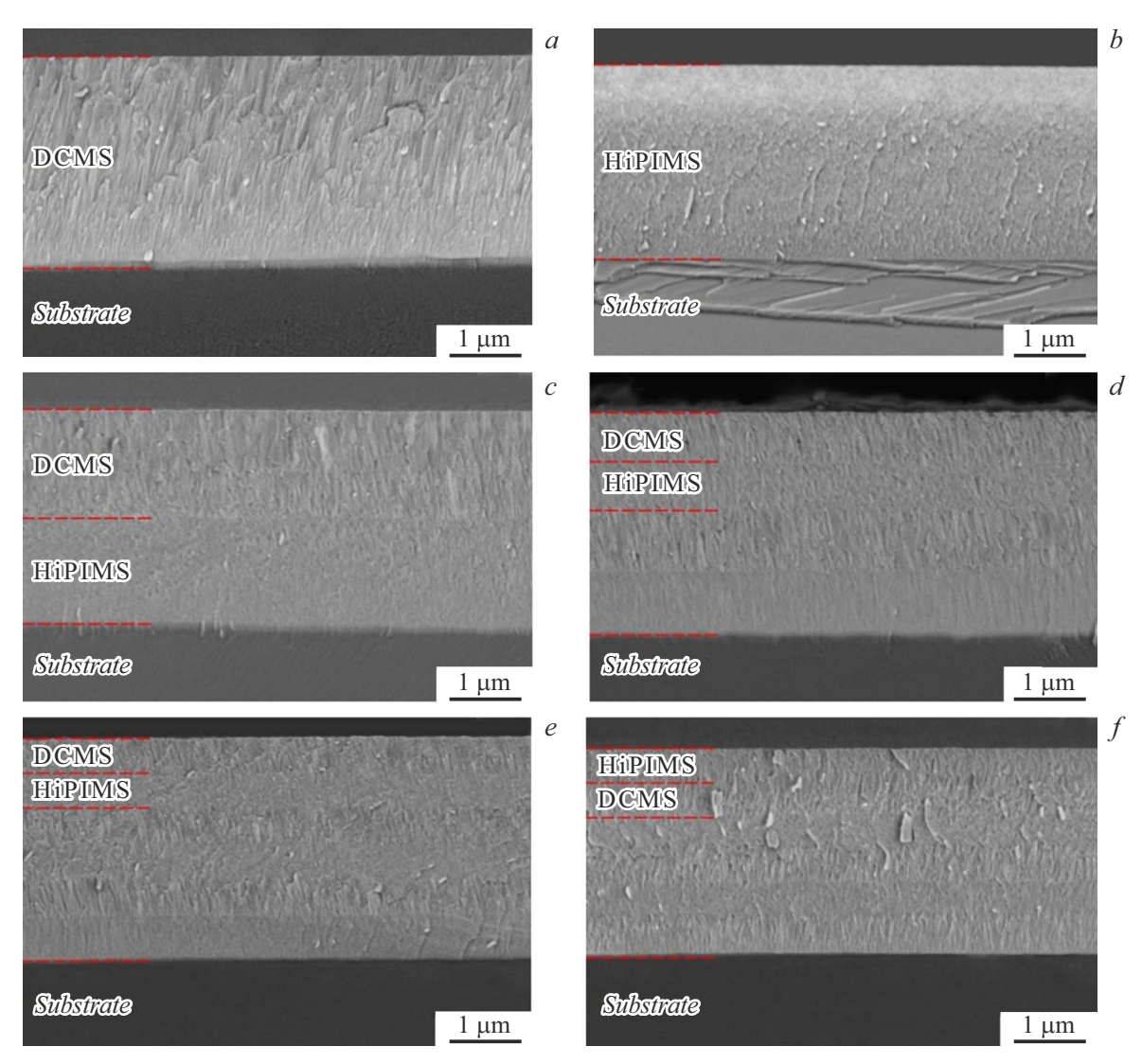


Figure 3. SEM images of the cross sections of the Ti-Al-Ta-N coatings produced in the various modes: a — D, b — H, c — HD2, d — HD4, e — HD6, f — DH6.

orientation, whereas the H coatings are characterized by a very strong texture (220). The predominant crystallite orientation in the direction (110) was previously detected in the TiN-based coatings that were applied either in the HiPIMS mode [21,22] or at high bias voltage applied to the substrate [21,23], i.e. when the growing coating is subjected to intense ion bombardment. In these conditions, the crystallographic texture of the coatings is determined by anisotropy of cascade collisions caused by ion bombardment [23,24]. In the crystallites, whose orientation ensures light channeling of the ions that bombard the growing coatings in the crystal lattice, their energy is dissipated in larger volumes, thereby reducing lattice distortions and probability of sputtering of adatoms. Therefore, these crystals have the least probability of sputtering and dominate during coating growth. Taking into account that the least-compactly packed planes of the crystal lattice in the NaCl structure are perpendicular to the direction (001), in the conditions of intense ion bombardment, depending on angular distribution of the incident ions, the TiN-based coatings usually have the textures (220) or (002) formed[24,25]. The diffraction patterns of the multilayer coatings are dominated by the peaks (111) and (220) that are related to the DCMS and HiPIMS layers, respectively.

Fig. 3 shows the average size of the coherent scattering regions d in the studied coatings. It can be seen from Table that in all the coatings produced using the HiPIMS mode, d is reduced as compared to the sample that is applied in the DCMS mode. The obtained data well comply with results of the previous studies which have shown that using the HiPIMS mode resulted in reduction of the crystallite size due to effects related to amplified ion bombardment [26]. At the same time, in the multilayer coatings d remained almost unchanged compared with the H coatings.

The microstructure of the cross sections of the coatings has been studied by means of SEM to show that the D coat-

Table 3. Average size of the coherent scattering regions d, the hardness H, the reduced Young's modulus E^* as well as the ratios H/E^* and H^3/E^{*2} of the Ti-Al-Ta-N coatings produced in the various modes

Designation of the coating batch	d, nm	H, GPa	E*, GPa	H/E^*	H^3/E^{*2}
D	12.42 ± 0.50	32.5 ± 1.3	330 ± 21	0.098	0.315
Н	7.72 ± 0.65	33.6 ± 1.5	324 ± 23	0.104	0.361
HD2	7.92 ± 0.72	32.7 ± 0.8	327 ± 15	0.100	0.327
HD4	8.14 ± 0.41	31.5 ± 1.8	308 ± 19	0.102	0.329
HD6	8.28 ± 0.55	32.5 ± 1.1	318 ± 16	0.102	0.339
DH6	8.66 ± 0.70	33.9 ± 0.9	329 ± 12	0.103	0.359

ings and the DCMS were characterized by a pronounced columnar structure, whereas the H coatings and the HiPIMS layers have a denser structure without columnar grains (Fig. 3). At the same time, the fracture surfaces of all the studied coatings did not exhibit defects pores and cracks.

Table 3 shows the hardness H and the reduced Young's modulus E^* of the Ti-Al-Ta-N coatings produced in the various modes of sputtering. The obtained data indicate that the highest hardness belongs to the H coatings (33.6 GPa) and the DH6 coatings (33.9 GPa), whereas the hardness of the other coatings is within 31.5-32.7 GPa. This effect can be explained by the fact that in the H and DH6 coatings the measured hardness is mainly contributed by layers that are produced in the HiPIMS mode and have a denser microstructure. At this, all the coatings have close values of the modulus of elasticity. Therefore, the H and DH6 coatings are also characterized by little higher values of H/E^* and H^3/E^{*2} (Table 3), which determine elastic and plastic strain limits of the materials, respectively [27,28].

The residual mechanical stresses have been measured to show that all the studied coatings exhibit development of compressive stresses, whose value remains constant within a measurement error (Fig. 4).

Fig. 5 shows variations of the coefficient of friction during tribological tests of the Ti-Al-Ta-N coatings in conditions of dry friction. It can be seen from the given graphs that an initial stage of the tests, when rubbing surfaces run in, exhibits sharp increase of the coefficient of friction due to increase of a real contact area, which is caused by fracture of microprotrusions on surfaces of the coatings and the counterbody. In 10 m of the tests, the coefficient of friction reaches values within the range 0.55-0.65 and with further tests it demonstrates only small fluctuations. At the stage of steady wear, all the studied coatings are characterized by close values of the coefficient of friction. At this, the highest average value of the coefficient of friction 0.70 belongs to the monolith H coatings, while the lowest value thereof 0.62 is observed for the D coatings. This effect can be explained by compaction of the microstructure of

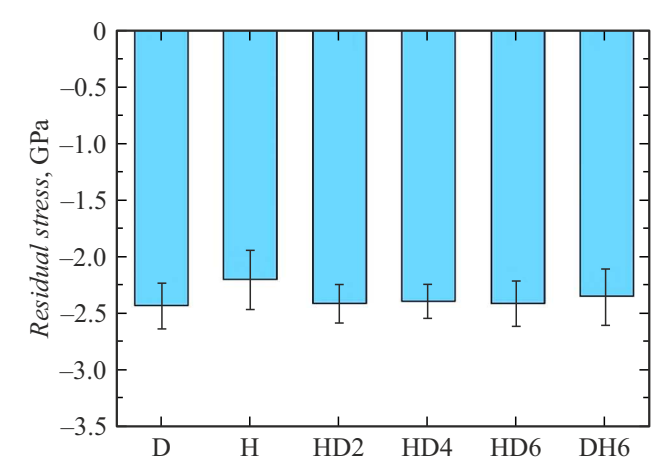


Figure 4. Residual stresses in the Ti-Al-Ta-N coatings produced in the various modes.

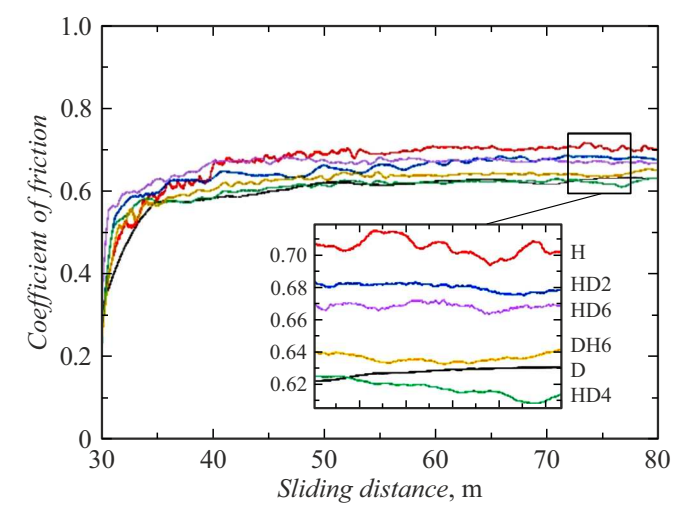


Figure 5. Dependence of the coefficient of friction of the Ti-Al-Ta-N coatings produced in the various modes, on a length of the friction path.

the Ti-Al-Ta-N coatings produced in the HiPIMS mode, which causes growth of the real contact area.

The tribotracks on the surface of the Ti-Al-Ta-N coatings were analyzed by means of SEM to show that their wear was predominantly of a abrasive-oxidative nature. Abrasive effect by the microprotrusions results in pitting of small particles of the coatings during cyclic loads. During further tests, a part of wear products is taken away from the tribotracks, whereas the wear particles that remain in a tribological contact area are destroyed and subjected to oxidation as a result of reaction with oxygen from the surrounding atmosphere. It can be seen from Fig. 6 that, as a result, the surface of the tribotracks exhibits formation of fragmented transfer layers, which consists of oxides of Ti, Al and Ta according to data of energy-dispersive spectroscopy. The presence of a considerable amount of oxygen causes darker contrast of these layers on the SEM images.

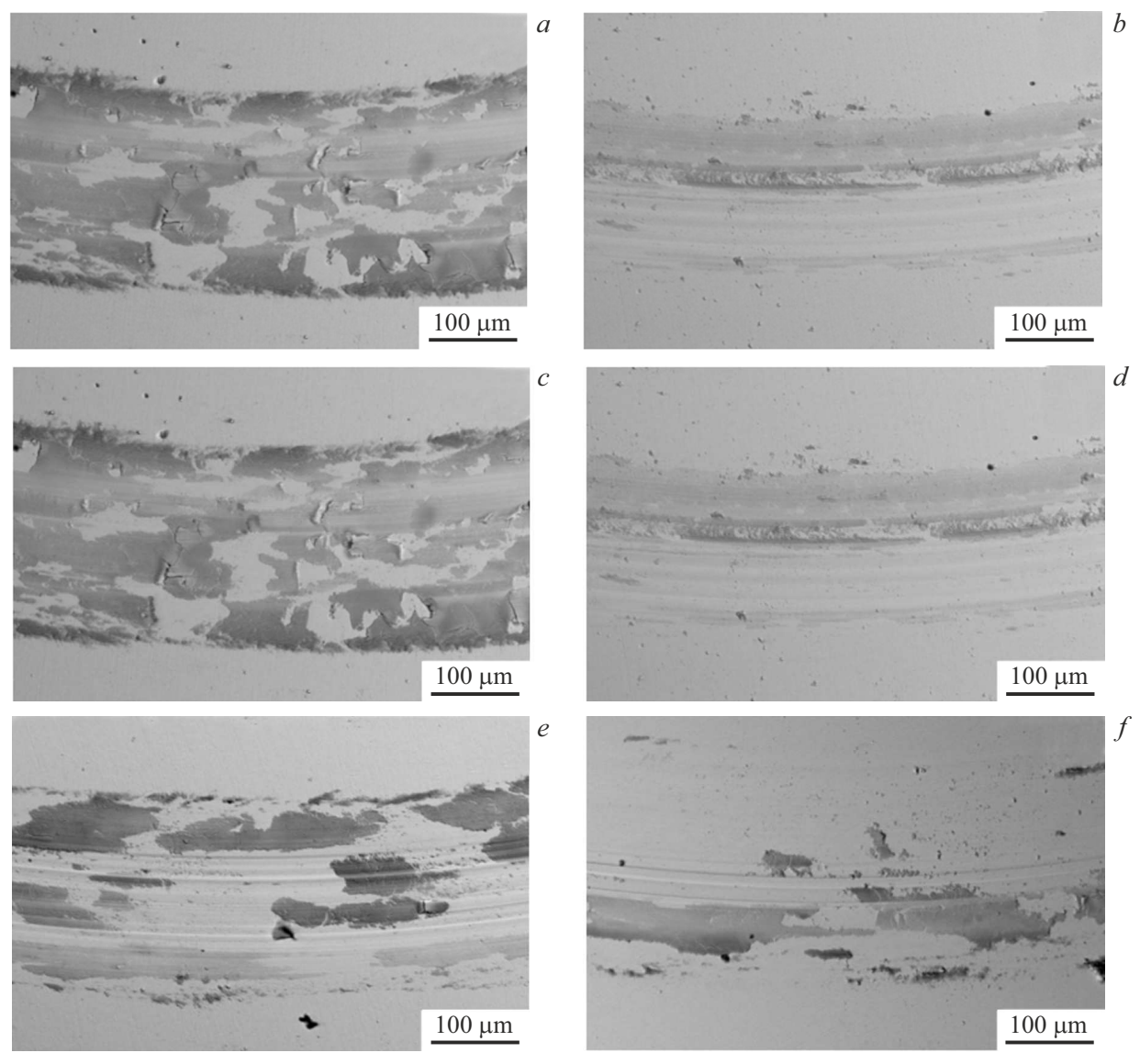


Figure 6. SEM images of the tribotracks on the surface of the Ti-Al-Ta-N coatings produced in the various modes: a — D, b — H, c – HD2, d — HD4, e — HD6, f — DH6.

Intensity of volume wear of the Ti-Al-Ta-N coatings has been evaluated by measuring the profiles of tribotracks that were formed at their surface after 100 m of the tribological tests, to show that maximum wear resistance belonged to the H coatings (Fig. 7). The intensity of wear of these coatings turned out to be by a factor of two less than for the D coatings. First of all, it is due to formation of the dense uniform microstructure without pronounced columnar grains in the H coatings, since boundaries between them are characterized by a reduced material density and, therefore, present ways for fast propagation of cracks during cyclic loading, thereby facilitating abrasive pitting of the coating particles. Wear resistance of the Ti-Al-Ta-N multilayer coatings turned out to be lower than for the H coatings, but higher than for the D coatings. The highest wear resistance among the multilayer compositions was demonstrated by the DH6 coatings, whose wear intensity was reduced by a factor of 1.5 as compared to the D coatings. Thus, the architecture of these coatings turned out to be the most preferable for ensuring high wear resistance, which is explained by the two main causes. First of all, there is a large number of interfaces between the layers, which more effectively suppress propagation of the cracks as compared to the 2- and 4-layer coatings. Secondly, each pair of layers of these coatings has the HiPIMS layer atop, which has higher wear resistance. Results of Fig. 7 have been compared to data of Table 3 to indicate that the ratios H/E^* and H^3/E^{*2} correlate well with intensity of wear of the Ti-Al-Ta-N coatings, thereby confirming applicability of these ratios for predic-

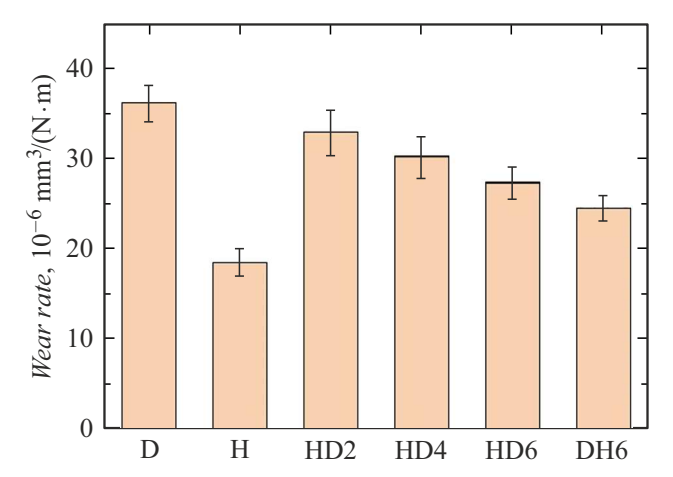


Figure 7. Intensity of wear of the Ti-Al-Ta-N coatings produced in the various modes.

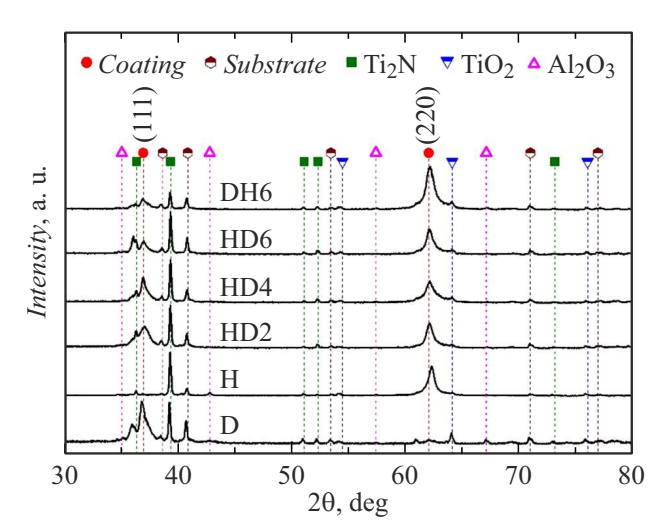


Figure 8. Diffraction patterns of the Ti-Al-Ta-N coatings produced in the various modes, after annealing for 5 h at the temperature of 950 °C.

In order to evaluate thermal stability and oxidation resistance of the Ti–Al–Ta–N coatings produced in the various modes, in the present study they were annealed in air atmosphere for 5h at the temperature of 950 °C. Fig. 8 shows the X-ray diffraction patterns obtained for the studied coatings. The diffraction patterns are analyzed to show that after annealing they still have peaks of the Ti–Al–Ta–N solid solution, whose intensity and location practically do not change as compared to the initial state. It indicates high thermal stability of the Ti–Al–Ta–N coatings. Besides, the diffraction patterns of all the coatings have reflections of the phases TiO₂ (rutile) and Ti₂N as well as weak peaks of corundum $(\alpha\text{-Al}_2\text{O}_3)$.

The microstructure of the cross sections of the annealed coatings has been analyzed to show that at the increased temperature they degrade in the same way (Fig. 9). A

surface of all the coatings has two-layer oxide formed after annealing. It can be seen from maps of distribution of the chemical elements, which are obtained by energy-dispersive spectroscopy, an upper, denser oxide layer of the thickness of less than 100 nm is enriched with Al, while a lower, porous layer is enriched with Ti and Ta (Fig. 10). The total thickness of the oxide layer is almost the same for all the studied coating and is 430-460 nm. Thus, despite the fact that the DCMS layers have columnar grains with open boundaries that can present ways for fast diffusion of oxygen inward the coatings, oxidation resistance of both the monolithic D coatings and the multilayer compositions with the top DCMS layer turned out to be no less than that of the H and DH6 coatings. It indicates that the process of oxidation of the Ti-Al-Ta-N coatings at the temperature of 950 °C is controlled not by kinetics of supply of oxygen to the oxide layer boundary, but kinetics of formation of the top protective Al₂O₃ layer, which prevents oxygen from entering the coating, as per the previous studies [29,30]. Along with formation of the oxide layer, all the studied sample exhibited formation of a porous diffusion layer at an interface between the coatings and the Ti-6Al-4V substrate. According to the energy-dispersive spectroscopy, this layer predominantly consists mainly of titanium and nitrogen (Fig. 10), with their relative content (at.%) being approximately 2:1. Taking into account results of X-ray diffraction, it can be assumed that this layer that was formed as a result of mutual diffusion between the coating and the substrate, consists of the Ti₂N phase.

Conclusion

The study has investigated the structure, the mechanical and tribological properties as well as oxidation resistance of the Ti-Al-Ta-N coatings produced in the various deposition modes. The performed studies have shown that using the combined HiPIMS/DCMS modes allowed increasing the deposition rate of the Ti-Al-Ta-N coatings by a factor of 1.5 as compared to the HiPIMS mode. It is found that increase of the number of the layers in the Ti-Al-Ta-N coatings contributes to increase of their hardness and wear resistance. At this, in terms of ensuring high values of hardness and wear resistance, more promising are the Ti-Al-Ta-N multilayer coatings, whose top layer is applied in the HiPIMS mode, thereby ensuring its denser microstructure. At the same time, creation of the multilayer architecture of the Ti-Al-Ta-N coatings using the combined HiPIMS/DCMS modes has no significant influence on their thermal stability and oxidation resistance, as these characteristics are predominantly controlled by the chemical composition of the coatings.

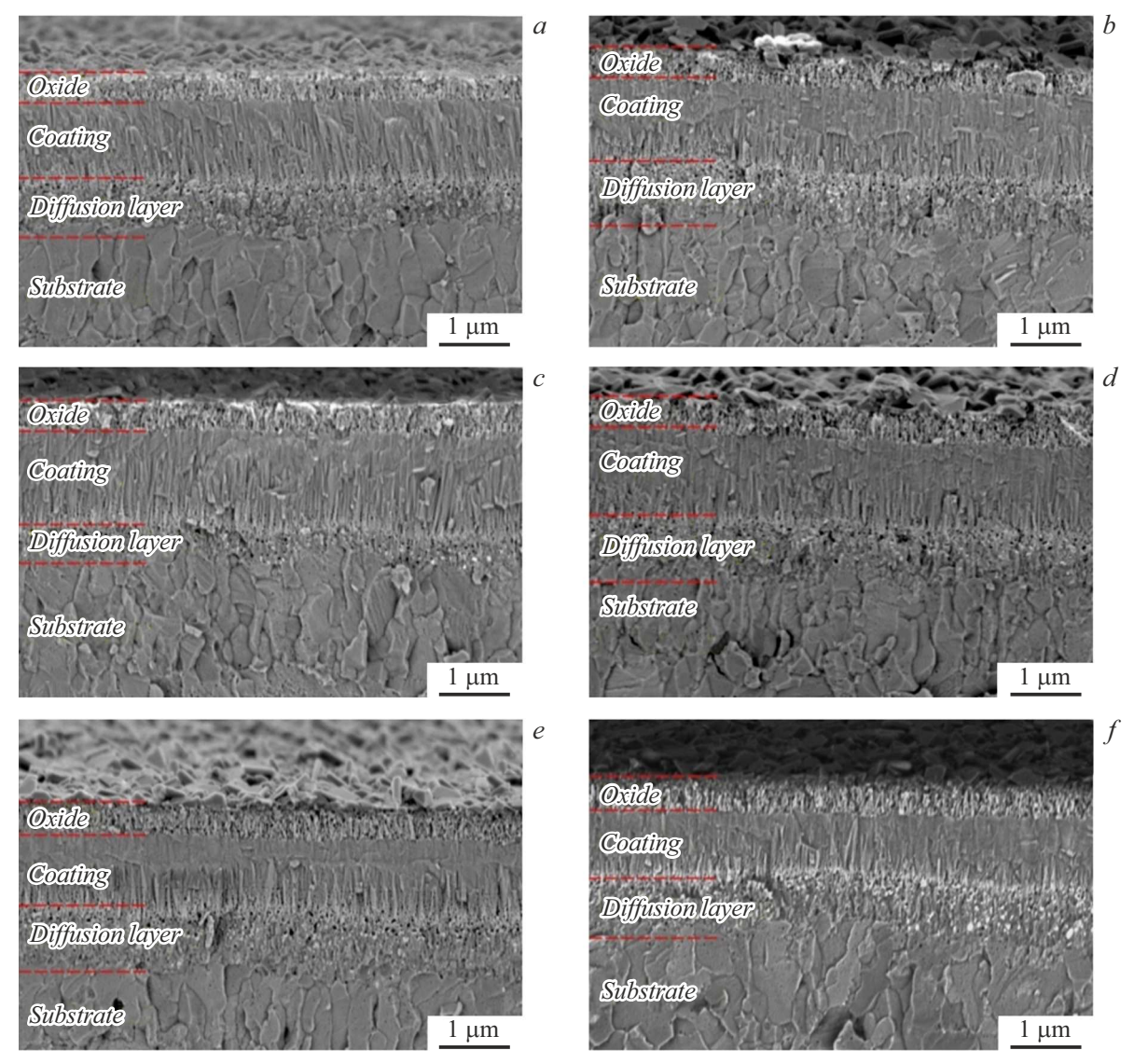


Figure 9. SEM images of the cross sections of the Ti-Al-Ta-N coatings on the Ti-6Al-4V substrates after annealing for 5 h at the temperature of 950 °C, as produced in the various modes: a - D, b - H, c - HD2, d - HD4, e - HD6, f - DH6.

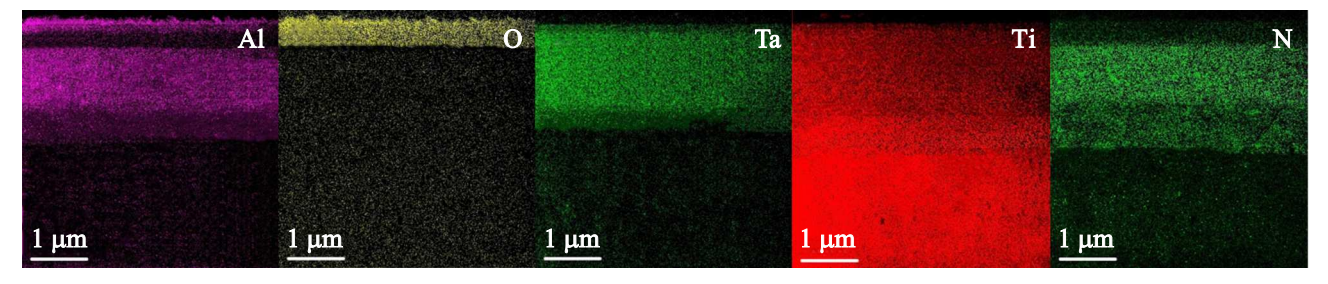


Figure 10. Maps of distribution of the chemical elements on the cross section of the coating produced in the DCMS mode on the VT6-alloy substrate after annealing at the temperature of 950° C for 5 h.

Funding

This study was carried out under the state assignment of the Institute of Strength Physics and Materials Science, SB RAS, project FWRW-2021-0010.

Acknowledgments

Equipment provided by the "Nanotech" Common Use Center of the Institute of Strength Physics and Materials Science, SB-RAS, and by Common Use Center of the Research and Development Center of NMNT TPU was used in the studies.

Conflict of interest

The authors declare that they have no conflict of interest.

References

- [1] D.G. Sangiovanni, V. Chirita, L. Hultman. Thin Solid Films, 520, 4080 (2012). DOI: 10.1016/j.tsf.2012.01.030
- [2] R. Rachbauer, D. Holec, P.H. Mayrhofer. Surf. Coat. Technol., 211, 98 (2012). DOI: 10.1016/j.surfcoat.2011.07.009.
- [3] S.V. Eremeev, A.R. Shugurov. Surf. Coat. Technol., 395, 125803 (2020). DOI: 10.1016/j.surfcoat.2020.125802
- [4] M. Mikula, M. Truchlý, D.G. Sangiovanni, D. Plasienka, T. Roch, M. Gregor, P. Durina, M. Janik, P. Kús. J. Vac. Sci. Technol. A, 35 (6), 060602 (2017). DOI: 10.1116/1.4997431
- [5] W.M. Seidl, M. Bartosik, S. Kolozsvari, H. Bolvardi, P.H. Mayrhofer. Vacuum, 150, 24 (2018). DOI: 10.1016/j.vacuum.2018.01.028.
- [6] A.R. Shugurov, E.D. Kuzminov, A.M. Kasterov, A.V. Panin,
 A.I. Dmitriev. Surf. Coat. Technol., 382, 125219 (2020).
 DOI: 10.1016/j.surfcoat.2019.125219
- [7] R. Hollerweger, H. Riedl, J. Paulitsch, M. Arndt, R. Rachbauer, P. Polcik, S. Primig, P.H. Mayrhofer. Surf. Coat. Technol., 257, 78 (2014).
 DOI: 10.1016/J.SURFCOAT.2014.02.067
- [8] M. Pfeiler, C. Scheu, H. Hutter, J. Schnöller, C. Michotte,
 C. Mitterer, M. Kathrein. J. Vac. Sci. Technol. A, 27, 554 (2009). DOI: 10.1116/1.3119671
- [9] C.M. Koller, S.A. Glatz, H. Riedl, S. Kolozsvári, P. Polcik,
 H. Bolvardi, P.H. Mayrhofer. Surf. Coat. Technol., 385, 125355 (2020). DOI: 10.1016/J.SURFCOAT.2020.125355
- [10] X. Sui, G. Li, C. Jiang, H. Yu, K. Wang, Q. Wang. Int. J. Refract. Met. Hard Mater., 58, 152 (2016). DOI: 10.1016/j.ijrmhm.2016.04.014
- [11] E. Contreras Romero, J. Cortínez Osorio, R. Talamantes Soto, A. Hurtado Macías, M. Gómez Botero. Surf. Coat. Technol., 377, 124875 (2019). DOI: 10.1016/J.SURFCOAT.2019.07.086
- Y. Choi, S. Jeon, J.M. Seok, S.H. Gyoo, H.H. Chun, Y. Lee,
 H. Lee. Appl. Surf. Sci., 258, 8752 (2012).
 DOI: 10.1016/j.apsusc.2012.05.086
- [13] W. Lü, G. Li, X. Li, S. Liu, J. Deng, Q. Wang. Ceram. Int., **50**, 920 (2024). DOI: 10.1016/j.ceramint.2023.10.177
- [14] W. Wang, G. Zhang, C. Wang, T. Wang, Y. Zhang, T. Xin.
 J. Alloys Compd., 946, 169385 (2023).
 DOI: 10.1016/j.jallcom.2023.169385
- [15] A.D. Korotaev, A.N. Tyumentsev. Phys. Mesomech., 26, 137 (2023). DOI: 10.1134/S1029959923020030
- [16] A.R. Shugurov, A.Y. Derbin, E.D. Kuzminov. Vacuum, 230, 113636 (2024). DOI: 10.1016/j.vacuum.2024.113636
- [17] A. Anders. J. Appl. Phys., 121 (171101), 1 (2017). DOI: 10.1063/1.4978350
- [18] G. Greczynski, S. Mráz, J.M. Schneider, L. Hultman. J. Appl. Phys., 127, 180901 (2020). DOI: 10.1063/1.5141342
- [19] P. Scherrer. GG-Nachrichten, 2, 98 (1918).
- [20] G.G. Stoney. Proc. R. Soc. Lond. Ser. A., **82**, 172 (1909). DOI: 10.1098/rspa.1909.0021
- [21] G.T.P. Azar, D. Er, M. Ürgen. Surf. Coat. Technol., 350, 1050 (2018). DOI: 10.1016/j.surfcoat.2018.02.066

- [22] H. Mei, J.C. Ding, X. Xiao, Q. Luo, R. Wang, Q. Zhang, W. Gong, Q. Wang. Surf. Coat. Technol., 405, 126514 (2021). DOI: 10.1016/j.surfcoat.2020.126514
- J.P. Zhao, X. Wang, Z.Y. Chen, S.Q. Yang, T.S. Shi, X.H. Liu.
 J. Phys. D: Appl. Phys., 30, 5 (1997).
 DOI: 10.1088/0022-3727/30/1/002
- [24] I. Petrov, L. Hultman, J.-E. Sundgren, J.E. Greene. J. Vac. Sci. Technol. A, 10, 265 (1992). DOI: 10.1116/1.578074
- [25] C.-H. Ma, J.-H. Huang, H. Chen. Thin Solid Films, 446, 184 (2004). DOI: 10.1016/j.tsf.2003.09.063
- [26] N.F.L. Dias, A.L. Meijer, D. Biermann, W. Tillmann. Surf. Coat. Technol., 487, 130987 (2024). DOI: 10.1016/j.surfcoat.2024.130987
- [27] A. Leyland, A. Matthews. Wear, 246, 1 (2000). DOI: 10.1016/S0043-1648(00)00488-9
- [28] J. Musil, F. Kunc, H. Zeman, H. Poláková. Surf. Coat. Technol., 154, 304 (2002).
 DOI: 10.1016/S0257-8972(01)01714-5
- [29] V. Khetan, N. Valle, D. Duday, C. Michotte, M.-P. Delplancke-Ogletree, P. Choquet. ACS Appl. Mater. Interfaces, 6, 4115 (2014). DOI: 10.1021/am405727p
- [30] A.R. Shugurov, A.V. Panin, A.M. Kasterov. Surf. Coat. Technol., 421, 127488 (2021).
 DOI: 10.1016/j.surfcoat.2021.127488

Translated by M.Shevelev